DOI:
10.1107/S2053230X20001466

Document Version
Peer reviewed version

Engineering the Fab fragment of anti-IgE omalizumab to prevent Fab and permit IgE-Fc complex crystallization

Authors

Alkistis N. Mitropoulou[ab], Tom Ceska[c], James T. Heads[c], Andrew J. Beavil[ab], Alistair J. Henry[c], James M. McDonnell[ab]*, Brian J. Sutton[ab]* and Anna M. Davies[ab]*

[a]Randall Centre for Cell and Molecular Biophysics, King's College London, New Hunt's House, London, SE1 1UL, UK

[b]Medical Research Council & Asthma UK Centre in Allergic Mechanisms of Asthma, London, UK

[c] UCB-Celltech, 208 Bath Road, Slough, SL1 3WE, UK

Correspondence email: james.mcdonnell@kcl.ac.uk; brian.sutton@kcl.ac.uk; anna.davies@kcl.ac.uk

Funding information Medical Research Council (grant No. G1100090 to Andrew J. Beavil, James M. McDonnell, Brian J. Sutton); Wellcome Trust (award No. 085944 to James M. McDonnell, Brian J. Sutton).

Synopsis The omalizumab Fab was engineered to disrupt recurring crystal packing interactions in Fab crystal structures; this led to the eventual structure determination of an omalizumab-derived Fab in complex with its target, IgE-Fc.

Abstract Immunoglobulin E (IgE) plays a central role in the allergic response, in which crosslinking of allergen by FcεRI-bound IgE triggers mast cell and basophil degranulation, and the release of inflammatory mediators. The high-affinity interaction between IgE and FcεRI is a long-standing target for therapeutic intervention in allergic disease. Omalizumab is a clinically approved anti-IgE monoclonal antibody that binds to free IgE, also with high affinity, preventing interaction with FcεRI. All attempts to crystallize the pre-formed complex between the omalizumab Fab and the Fc region of IgE (IgE-Fc), to understand the structural basis for its mechanism of action, surprisingly failed. Instead, the Fab alone selectively crystallized, in different crystal forms, but their structures revealed intermolecular Fab/Fab interactions that were clearly strong enough to disrupt the Fab/IgE-Fc complexes. Some of these interactions were common to other Fab crystal structures. We therefore designed mutations to disrupt two recurring packing interactions observed in the omalizumab Fab crystal structures, without interfering with the ability of the omalizumab Fab to recognize IgE-Fc; this led to the successful crystallization and subsequent structure determination of the Fab/IgE-Fc complex. The mutagenesis strategy adopted to achieve this result is applicable to other intractable Fab/antigen complexes or systems in which Fabs are used as crystallization chaperones.

Keywords: Omalizumab; allergy; Immunoglobulin E (IgE); Fab; antibody; protein engineering; X-ray crystallography.

1. Introduction

Immunoglobulin E (IgE) plays a central role in allergic disease through the interaction between its Fc region (IgE-Fc) and the FcεRI receptor, in which cross-linking of FcεRI-bound IgE by allergen triggers mast cell and basophil degranulation, with the release of inflammatory mediators (Gould & Sutton, 2008).

IgE-Fc, comprising two identical disulphide-linked chains of Cε2, Cε3 and Cε4 domains, adopts a bent conformation in solution (Beavil *et al*., 1995; Davis *et al*., 1990; Holowka & Baird, 1983; Holowka *et al*., 1985; Hunt *et al*., 2012; Zheng *et al*., 1991; Zheng *et al*., 1992). In the crystal structure of unbound IgE-Fc, the Fc region is acutely bent: the $(Cε2)_2$ domain pair folds back against the Cε3 and Cε4 domains, with an angle of 62° between the local two fold axes of the Cε2 and Cε4 domain pairs (Doré *et al*., 2017; Holdom *et al*., 2011; Wan *et al*., 2002). The Fcε3-4 region, comprising only the Cε3 and Cε4 domains, is conformationally flexible, and the Cε3 domains can adopt a variety of positions relative to one another, from "closed" to "open" (Chen *et al*., 2018; Cohen *et al*., 2014; Davies *et al*., 2017; Dhaliwal *et al*., 2012; Dhaliwal *et al*., 2014; Dhaliwal *et al*., 2017; Doré *et al*., 2017; Drinkwater *et al*., 2014; Garman *et al*., 2000; Holdom *et al*., 2011; Jabs *et al*., 2018; Wan *et al*., 2002; Wurzburg & Jardetzky, 2009; Wurzburg *et al*., 2000; Yuan *et al*., 2013), a property associated with the mutually exclusive, allosteric regulation of binding to FcεRI and the second principal receptor for IgE, CD23 (Borthakur *et al*., 2012; Dhaliwal *et al*., 2012). The Cε3 domains adopt an open conformation, and IgE-Fc becomes more acutely bent, when in complex with FcεRI (Garman *et al*., 2000; Holdom *et al*., 2011; Hunt *et al*., 2012), while CD23 binds when the Cε3 domains adopt a closed conformation (Dhaliwal *et al*., 2012; Dhaliwal *et al*., 2014; Dhaliwal *et al*., 2017; Yuan *et al*., 2013). The potential for more extreme flexibility in IgE-Fc was first revealed when a fully extended, linear structure, involving a ~120° unbending of the $(Cε2)_2$ domain pair relative to the Fcε3-4 region, was captured by an anti-IgE Fab (Drinkwater *et al*., 2014). Molecular dynamics simulations have also revealed that IgE-Fc can adopt relatively stable, partially bent conformations, in between the two extremes of acutely bent and fully extended (Drinkwater *et al*., 2014).

The high-affinity interaction between IgE and FcεRI is a long-standing target in the development of treatments for allergic disease (Holgate, 2014). Omalizumab is an anti-IgE therapeutic monoclonal IgG1 antibody that inhibits the interaction with FcεRI, and is approved for the treatment of moderate-to-severe persistent allergic asthma and chronic idiopathic urticaria (Holgate *et al*., 2005; Sussman *et al*., 2014). Although the binding site of omalizumab had previously been mapped to the Cε3 domain (Zheng *et al*., 2008), and omalizumab was known to bind to a partially bent IgE-Fc conformation

(Hunt *et al*., 2012), the structural basis for its mechanism of action was poorly understood until only recently.

We, and others (Jensen *et al*., 2015), had attempted to crystallize the complex between the omalizumab Fab and IgE-Fc. However, despite extensive efforts, our crystallization trials of pre-formed omalizumab Fab/IgE-Fc and Fcε3-4 complexes only resulted in selective crystallization of the Fab. The structure of the omalizumab Fab in complex with the Fcε3-4 region of IgE-Fc has been reported, which revealed details of the omalizumab epitope on the Cε3 domain (Pennington *et al*., 2016). However, this Fcε3-4 molecule lacked the $(C\varepsilon2)_2$ domain pair and was conformationally constrained by an engineered disulphide bond that locked the Cε3 domains into a closed conformation (Pennington *et al*., 2016). Given the flexible nature of the Fcε3-4 region, and the potential for extreme flexibility in IgE-Fc, which additionally contains the $(C\varepsilon2)_2$ domain pair, this structure could thus provide only limited mechanistic insights.

We designed a mutagenesis strategy to disrupt the packing interactions observed in omalizumab Fab crystal structures, without affecting the antigen-binding CDRs, with the aim of crystallizing the complex between the omalizumab Fab and IgE-Fc. The strategy first involved creating a point mutation in a short segment of β-strand structure found in the Cκ domain CD loop, followed by two point mutations in the V_L domain EF loop.

One omalizumab-derived Fab, termed FabXol3, which contains three point mutations in the light chain, later enabled us to solve the 3.7Å resolution crystal structure of the complex with IgE-Fc, revealing that omalizumab inhibits binding to FcεRI allosterically (Davies *et al*., 2017). In this complex, IgE-Fc adopts a partially bent conformation, and the Cε3 domains adopt a markedly open conformation, more open than that seen in any other crystal structure thus far.

Here we report the structural basis and rationale for this mutagenesis strategy. Such an approach could inform the design and structure determination of other Fabs in complex with their target proteins in cases where the pre-formed complex is disrupted by selective crystallization of one partner, in particular the Fab.

2. Materials and methods

2.1. Macromolecule production

IgE-Fc, Fcε3-4, FabXol, FabXol2, FabXol3 and scFvXol proteins were produced using previously described methods (Davies *et al*., 2017; Dhaliwal *et al*., 2012; Drinkwater *et al*., 2014; Weatherill *et al*., 2012; Young *et al*., 1995). Omalizumab was purchased from Novartis Europharm Limited.

2.2. Crystallization

All crystals were grown at 18°C using the sitting drop vapour diffusion method in MRC 96 well plates. FabXol[1] and FabXol[2] (omalizumab Fab) crystals were grown from unsuccessful crystallization trials of the FabXol/IgE-Fc and FabXol/Fcε3-4 complexes. For the FabXol[1] and FabXol[2] structures reported here, the 2:1 complex between FabXol and Fcε3-4 was purified by size exclusion chromatography, buffer exchanged to 25mM Tris-HCl pH7.5 and 20mM NaCl, and concentrated to 18.8 mg/mL. FabXol[1] crystals were grown in 0.085M Tris pH8.5, 42.5% (v/v) MPD, 15% glycerol (v/v) and 0.17M ammonium phosphate, and cryoprotected with mother liquor. FabXol[2] crystals were grown in 0.1M phosphate-citrate pH4.2, 20% (w/v) PEG 1000 and 0.2M lithium sulphate, and cryoprotected with 0.1M sodium acetate pH4.6, 25% (w/v) PEG 4000 and 18% (v/v) ethylene glycol. For both crystals, a reservoir volume of 50µL was used, and the drops comprised 100nL protein and 200nL reservoir solution.

FabXol1[1] and FabXol1[2] (omalizumab-derived Leu158Pro light chain mutant Fab) crystals were grown from unsuccessful crystallization trials of the FabXol1/IgE-Fc complex. The 2:1 complex between FabXol1 and IgE-Fc was purified by size exclusion chromatography, buffer exchanged into 0.25M Tris-HCl pH7.5 and 0.2M NaCl, and concentrated to 18.8 mg/mL. FabXol1[1] crystals were grown in 20% (w/v) PEG 3350 and 0.2M sodium sulphate, and were cryoprotected with 20% (w/v) PEG 3350, 0.2M magnesium sulphate and 18% (v/v) ethylene glycol. FabXol1[2] crystals were grown in 20% (w/v) PEG 4000, 0.2M magnesium sulphate and 10% (v/v) glycerol, and cryoprotected in 20% (w/v) PEG 4000, 0.2M magnesium sulphate and 18% (v/v) glycerol. For both crystals, a reservoir volume of 50µL was used, and the drops comprised 100nL protein and 200nL reservoir solution.

FabXol2 (omalizumab-derived Ser81Arg, Gln83Arg light chain mutant Fab) was buffer exchanged into 0.1M Tris-HCl pH8.5 and 0.05M NaCl, and concentrated to 3mg/mL. FabXol2 crystals were grown in 0.1M HEPES pH7 and 20% (w/v) PEG 4000, and cryoprotected with 12% (v/v) PEG 400 and 17% (v/v) glycerol; a reservoir volume of 100µL was used, and the drops comprised 200nL

protein and 100nL reservoir. FabXol3 (omalizumab-derived Ser81Arg, Gln83Arg, Leu158Pro light chain mutant Fab) was purified in PBS and concentrated to 15mg/mL, then diluted to 5mg/mL with 0.1M Tris pH8.5. FabXol3 crystals were grown in 0.1M HEPES pH7, 20% (w/v) PEG 4000 and 0.15M ammonium sulphate, and cryoprotected with 0.1M HEPES pH7.5, 20% (w/v) PEG 4000, 0.1M ammonium sulphate and 15% (v/v) ethylene glycol; a reservoir volume of 50μL was used, and the drops comprised 100nL protein and 200nL reservoir solution. scFvXol was buffer exchanged into 0.25M Tris-HCl pH8.5 and 0.2M NaCl, and concentrated to 3.9mg/mL. scFvXol crystals were grown in 0.1M tri-sodium citrate pH5.6, 15% (w/v) PEG 4000 and 0.2M ammonium sulphate, and cryoprotected with 0.1M tri-sodium citrate pH5.6, 30% (w/v) PEG 4000 and 0.2M ammonium sulphate; a reservoir volume of 100μL was used, and the drops comprised 100nL protein and 80nL reservoir solution.

2.3. X-ray data collection, processing, structure determination and refinement

Data were collected at beamlines I02, I03, I04, I04-1 and I24 at the Diamond Light Source (Harwell, UK). Data were integrated with XDS (Kabsch, 2010) using the xia2 package (Winter, 2010), or MOSFLM (Leslie & Powell, 2007), and scaled with AIMLESS (Evans & Murshudov, 2013) or SCALA (Evans, 2006) from the CCP4 suite (Winn *et al*, 2011). Structures were solved by molecular replacement using MOLREP (Vagin & Teplyakov, 1997) or PHASER (McCoy *et al*., 2007). Protein atoms from PDB ID: 2FJF (Fuh *et al*., 2006) were used as a search model for the FabXol[1] structure. Subsequent structures were solved using protein atoms (V_H, V_L, Cκ and Cγ1 domains) from the FabXol[1] structure as a search model, although CDR residues were removed. Structures were initially refined with REFMAC (Murshudov *et al*., 2011), and later with PHENIX (Adams *et al*., 2010), and refinement was alternated with rounds of manual model building with Coot (Emsley *et al*., 2010). Model quality was assessed with MolProbity (Chen *et al*., 2010). Data processing and refinement statistics are summarized in Tables 1 and 2. Interfaces were analysed with PISA (Krissinel & Henrick, 2007). Figures were produced with PyMOL.

2.4. PDB references

Coordinates and structure factors have been deposited at the Protein Data Bank with accession codes: FabXol[1], 6TCM; FabXol[2], 6TCN; FabXol1[1], 6TCO; FabXol1[2], 6TCP; FabXol2, 6TCQ, FabXol3, 6TCR; scFvXol, 6TCS.

2.5 Fluorescence based thermal stability (T_m) measurement

A thermal stability assay was performed using a QuantStudio 7 Real-Time PCR System (Thermo Fisher). 5µL of 30x SYPRO™ Orange Protein Gel Stain (Thermo Fisher), diluted from 5000x concentrate with PBS pH7.4, was added to 45µL of protein sample (0.2mg/mL in PBS pH7.4), and mixed. 10µL of this solution was dispensed into a 384 PCR optical well plate. The PCR heating device was set at 20°C and increased to 99°C at a rate of 1.1°C/min. A charge-coupled device was used to monitor fluorescence changes in the wells. Fluorescence intensity increases were plotted, the inflection point of the slope was used to generate apparent midpoint temperatures (T_m).

2.6. Surface plasmon resonance

Surface plasmon resonance binding experiments were performed using a Biacore T200 instrument (GE Healthcare). Intact omalizumab, the Fabs and scFv were immobilised at similar densities on CM5 sensor chips, using an amine coupling protocol according to the manufacturer's instructions (GE Healthcare). The following immobilization densities were used for these studies: omalizumab, 970 resonance units; FabXol, 200 resonance units; FabXol2, 270 resonance units; FabXol3, 210 resonance units and scFvXol, 250 resonance units. For binding studies, IgE-Fc, in a two-fold dilution series (100-0.4nM) was injected at a flow rate of 20µL/min for 240s, followed by a dissociation time of 900s. All binding experiments were performed at 25°C in 20mM HEPES pH7.4, 150mM NaCl and 0.005% (v/v) surfactant P20. Biaevaluation (GE Healthcare) and Origin 8 (OriginLab) were used to analyse and present the data. For a visual comparison of IgE-Fc binding curves to the different omalizumab constructs, the 100nM concentration for each was adjusted to give a maximal binding of 100 resonance units and these curves were overlaid.

3. Results

The nomenclature used for the omalizumab-derived Fabs and scFv reported here, and their crystal structures, is presented in Table 3. Heavy and light chain CDRs are defined as follows: CDRH1, Ser25-Asn36; CDRH2, Ser51-Asn59; CDRH3, Ala97-Val110; CDRL1, Arg24-Asn38; CDRL2, Tyr53-Ser60; CDRL3, Gln93-Thr101 (North *et al*., 2011).

3.1. Crystal structures of FabXol (wild-type omalizumab Fab) – FabXol^1 and FabXol^2

The structure of FabXol (wild-type omalizumab Fab) was solved in two different crystal forms, which have also been reported by others (Jensen *et al*., 2015; Wright *et al*., 2015), and the space group and unit cell parameters for these structures, FabXol^1 and FabXol^2, the latter now reported at substantially

higher resolution, are provided in Table 1. The structures reported here were the result of unsuccessful crystallization trials of the complex between FabXol and an unconstrained Fcε3-4 molecule, but similar crystals were also grown from crystallization trials of FabXol in complex with IgE-Fc.

The FabXol[1] structure (1.85Å resolution) contains one Fab in the asymmetric unit, which forms two distinct interfaces with symmetry-related molecules (Fig. 1*a*). At the first interface, an area of ~395Å^2, residues from all three heavy chain CDRs contact V_L and Cκ domain framework residues from a symmetry-related molecule; namely, the V_L domain AB, C''D and EF loops, and the Cκ domain DE loop. In addition to van der Waals interactions, this interface comprises four hydrogen bonds, namely Thr30 (CDRH1) – Ser81 (V_L), Ser31 (CDRH1) – Asp17 (V_L), Tyr54 (CDRH2) – Arg65 (V_L), and Tyr102 (CDRH3) – Ser175 (Cκ) (Fig. 1*b*).

The second interface, an area of ~324Å^2, includes an extensive network of hydrogen bonds between an edge β-strand from the Cγ1 domain (β-strand G) and a short segment of β-strand structure in the Cκ domain CD loop from a symmetry-related molecule. Here, the β-strands are arranged in a parallel manner, with hydrogen bonds between main chain atoms from Lys214-Lys218 (Cγ1) and Leu158-Ser160 (Cκ), and the side chains of Lys217 (Cγ1) and Ser160 (Cκ) (Fig. 1*c*). This interface is repeated throughout the crystal lattice, as an identical interface forms between Leu158-Ser160 (Cκ) and Lys214-Lys218 (Cγ1) from a symmetry-related molecule.

The FabXol[2] structure (2.3Å resolution) contains two Fab molecules in the asymmetric unit, referred to here as FabXol^{2A} and FabXol^{2B}. The CDRs from both molecules adopt similar conformations to those observed in the FabXol[1] structure. CDRH1-3 residues also interact with V_L and Cκ domain framework residues, akin to the first interface observed in the FabXol[1] structure, which, for FabXol^{2B}, also includes a hydrogen bond between His101 (CDRH3) and Gln83 (V_L) (Fig. 1*d*). The arrangement of Fabs in the FabXol[2] asymmetric unit precludes propagation of the second, β-strand mediated interface throughout the crystal lattice by a single Fab molecule, as in the FabXol[1] structure. However, interactions between FabXol^{2A} and FabXol^{2B}, and different symmetry-related molecules, each display this same β-strand interaction, in which Lys214-Lys218 (Cγ1) from FabXol^{2A} interact with Leu158-Ser160 (Cκ) from one symmetry-related molecule, while Leu158-Ser160 (Cκ) from FabXol^{2B} interact with Lys214-Lys218 (Cγ1) from a different symmetry-related molecule.

3.2. Crystal structure of scFvXol (omalizumab-derived scFv)

We also attempted to crystallize the complex between a single-chain form of omalizumab (scFvXol) and IgE-Fc, but were unsuccessful. However, we solved the crystal structure of scFvXol alone, in which the light and heavy chain variable domains are connected by a $(Gly_4Ser)_4$ linker, to 2.3Å resolution (Table 1). The scFvXol structure contains one molecule in the asymmetric unit.

In this structure, the β-strand mediated crystal packing interaction observed in the FabXol[1] and FabXol[2] structures is absent, as the construct lacks the Cγ1 and Cκ domains. However, CDRH1-3 residues from a symmetry-related molecule contact the V_L domain of scFvXol in a similar manner to the first interface described for the FabXol[1] and FabXol[2] structures, although the interface area is reduced from ~395A^2 to ~290Å^2 due to the absence of the Cκ domain in scFvXol.

3.3. Mutagenesis strategy I - disrupting the interaction between Cγ1 and Cκ domains

Crystallization trials of the complexes between FabXol (omalizumab Fab) and IgE-Fc, scFvXol (omalizumab-derived scFv) and IgE-Fc, and FabXol and an unconstrained Fcε3-4 molecule, all led to selective crystallization of the Fab, or were unsuccessful. Two recurring interfaces in the Fab and scFvXol structures, described in section 3.1, suggested a route to disrupt crystal packing interactions, without mutating the CDR residues responsible for IgE-Fc binding.

We first attempted to disrupt the interface between the edge β-strand (β-strand G) from the Cγ1 domain (Lys214-Lys218) and the short β-strand segment in the Cκ domain CD loop (Leu158-Ser160), observed in the FabXol[1] and FabXol[2] structures. Leu158 from the Cκ domain CD loop was mutated to proline, with the aim of altering its secondary structure, to disrupt the extensive, hydrogen-bond mediated interactions. This omalizumab-derived Leu158Pro mutant Fab was termed FabXol1.

3.4. Crystal structures of FabXol1 (omalizumab-derived Leu158Pro mutant Fab) – FabXol1[1] and FabXol1[2]

The Leu158Pro mutation alone was not sufficient to prevent selective crystallization of the Fab, and the structures reported here were the result of unsuccessful crystallization trials of the complex

between FabXol1 and IgE-Fc. Two structures were solved for FabXol1, in new crystal forms, and the space group and unit cell parameters for these structures, FabXol1[1] and FabXol1[2], are provided in Table 2.

The FabXol1[1] structure (1.8Å resolution) contains two Fab molecules (FabXol1[1A/B]) in the asymmetric unit (Fig. 2*a*). In this structure, the network of hydrogen bonds observed in the FabXol structures between β-strands of the Cγ1 and Cκ domains is indeed disrupted, but the engineered residue, Pro158, now forms other crystal packing interactions.

In molecule FabXol1[1A], Asp155-Gln159, and His193 (Cκ), including Pro158, form an interface with Pro62, Lys65-Arg67 and Arg87 (V_H) from a crystallographic symmetry-related molecule, burying a surface area of 187Å^2 (Fig. 2*b*). In molecule FabXol1[1B], Lys149, Gln151, Lys153, Asn156, Pro158-Gly161, and Glu199 (Cκ), form an interface of 215Å^2 with Gly161, Ser163 and Gln164 (Cκ), Ala88 and Glu89 (V_H), and Leu178-Gly182 (Cγ1) from the non-crystallographic symmetry-related molecule, FabXol1[1A] (Fig. 2*c*).

CDRH1-3 residues from both molecules of the FabXol1[1] structure adopt essentially identical conformations to those found in the FabXol[1] and FabXol[2] (wild-type omalizumab Fab) and scFvXol (omalizumab-derived scFv) structures. These form similar crystal packing interactions to the first interface described for the FabXol[1] structure, in which the heavy chain CDRs contact the V_L domain AB, C''D and EF loops, and Cκ domain DE loop from a symmetry-related molecule. In both molecules, hydrogen bonds form between Ser31 (CDRH1) - Asp17 (V_L), Tyr54 (CDRH2) - Arg65 (V_L) and Tyr102 (CDRH3) – Ser175 (Cκ) (Fig 2*d*).

The FabXol1[2] structure (2.5Å resolution) contains four Fab molecules (FabXol1[2A-D]) in the asymmetric unit. In this structure, the packing environment of Pro158 differs from that in the FabXol1[1] structure. Again, the β-strand interactions between Cγ1 and Cκ are disrupted, but new packing interactions involving Pro158 are formed. In all four molecules of the FabXol1[2] structure, Pro158 forms van der Waals interactions with Pro158-Ser160 (Cκ) from a non-crystallographic symmetry-related Fab (Fig. 3*a*). In this manner, Pro158 mediates light-chain/light-chain interactions between FabXol1[2A] and FabXol1[2C], and between FabXol1[2B] and FabXol1[2D]. Due to the arrangement of the four Fab molecules in the asymmetric unit, Pro158 from FabXol1[2C] is positioned at an interface comprising three Fabs (FabXol1[2A-C]), and in addition to the interface with Pro158-Ser160 from FabXol1[2A], also contacts Arg87 (V_H) from FabXol1[2B] (Fig. 3*a*).

In molecules FabXol1[2A] and FabXol1[2B], the heavy chain CDRs adopt similar conformations to those in the FabXol, scFvXol and FabXol1[1] structures. CDR residues from FabXol1[2B] form a similar interface with V_L and Cκ domain framework residues from a symmetry-related molecule; hydrogen bonds form between Ser31 (CDRH1) - Asp17 (V_L), Tyr54 (CDRH2) - Arg65 (V_L), His101 (CDRH3) - Gln83 (V_L) and Tyr102 (CDRH3) - Ser175 (Cκ), burying a surface area of 384Å^2. Although FabXol1[2A] contacts the V_L and Cκ domains from a symmetry-related molecule, the position of this molecule is shifted, and the interface area, reduced to 274Å^2, contains a single hydrogen bond between Tyr102 (CDRH3) and Asp174 (Cκ) (Fig. 3*b*).

By contrast, the CDRH1 and CDRH3 conformations differ in molecules FabXol1[2C] and FabXol1[2D], compared with the other structures described thus far. In these molecules, binding of a glycerol molecule causes the Tyr33 (CDRH1) and His101 (CDRH3) side chains to adopt substantially different positions (Fig. 3*c*), the implications of which are discussed later. Crystal contacts for FabXol1[2C] and FabXol1[2D] also differ markedly compared with the other Fabs. In FabXol1[2C], Thr30 and Ser31 (CDRH1) form hydrogen bonds with Thr73 and Ser28 (V_L), respectively, from one symmetry-related molecule, while Tyr102 (CDRH3) packs against Gly15 and Gly16 (V_H) from another (Fig. 3*d*). On the other hand, in FabXol1[2D], only the interaction between Tyr102 and Gly15 and 16 from the second symmetry-related molecule is found; the first molecule is positioned further away, precluding hydrogen bonds between Thr30 and Ser31 (CDRH1), and Thr73 and Ser28, respectively. By contrast, CDRH2 residues do not participate in any crystal contacts, and adopt similar conformations to those in FabXol1[2A] and FabXol1[2B].

Despite the different contacts formed by CDRH1 and CDRH3 in molecules FabXol1[2C] and FabXol1[2D], the packing environment would not preclude the CDR conformations observed in the FabXol, scFvXol, FabXol1[1] structures, and molecules FabXol1[2A] and FabXol1[2B].

3.5. Mutagenesis strategy II - disrupting packing interactions involving the heavy chain CDRs

Although the Leu158Pro mutation in the short β-strand segment of the Cκ domain CD loop disrupted the interaction with the Cγ1 domain edge β-strand (strand G), it did not prevent selective crystallization of the Fab. We next attempted to disrupt the interface between the heavy chain CDRs, and V_L and Cκ domain framework residues. As most of this interface involves interactions between the CDRs and the V_L domain, and mutating the CDRs could adversely affect the interaction with IgE-

Fc, we mutated Ser81 and Gln83 from the V_L domain EF loop, which contribute to this interface, to Arg81 and Arg83, respectively, thus incorporating bulkier, charged side chains. We created two omalizumab-derived Fabs, namely FabXol2, with Ser81Arg and Gln83Arg mutations, and FabXol3, which additionally contains the Leu158Pro mutation. Thermal stability measurements revealed that incorporation of these three point mutations, either alone or in combination with one another, did not affect the overall stability of the Fabs (Table 4).

3.6. Crystal structures of FabXol2 (omalizumab-derived Ser81Arg, Gln83Arg mutant Fab) and FabXol3 (omalizumab-derived Ser81Arg, Gln83Arg, Leu158Pro mutant Fab)

Complexes between IgE-Fc and both the omalizumab-derived Fabs that contained the Ser81Arg and Gln83Arg mutations were eventually crystallized. Crystals with a similar morphology were grown for each complex, although the FabXol3/IgE-Fc complex crystals diffracted to higher resolution, and we recently reported the crystal structure of the complex to 3.7Å resolution (Davies *et al*., 2017).

To understand the effects of the Ser81Arg and Gln83Arg (V_L) mutations on Fab crystal packing interactions, we solved the structures of FabXol2 and FabXol3 alone. Both FabXol2 and FabXol3 crystallized in the same crystal form (Table 2), with one Fab molecule in the asymmetric unit. With the exception of the light chain residue 158, which is leucine in FabXol2 and proline in FabXol3, the structures are otherwise essentially identical.

The packing interactions that involve V_L domain residues 81 and 83 in the FabXol and FabXol1 structures are substantially different in the FabXol2 and FabXol3 structures. In contrast to Ser81, which contacts Ser31 (CDRH1) and Tyr54 (CDRH2), Arg81 instead forms hydrogen bonds with Asn156 (Cκ, symmetry-related molecule) (Fig. 4*a*). In FabXol3, Arg81 contacts Pro158 (Cκ), while Leu158 is partially disordered in FabXol2. Furthermore, and in contrast to Gln83, which contacts Tyr33 (CDRH1), Tyr54 (CDRH2), and His101 (CDRH3) in the FabXol and FabXol1 structures, Arg83 does not participate in any crystal packing interactions in the FabXol2 and FabXol3 structures (Fig. 4*a*). As the overall structures for FabXol2 and FabXol3 are similar, further discussion will be limited to the FabXol3 structure, solved at higher resolution (1.45Å for FabXol3 compared with 2.05Å for FabXol2).

In the FabXol3 structure, CDRH1 and CDRH3 residues contact the V_L domain of one symmetry-related molecule at an interface that includes hydrogen bonds between Ser31 (CDRH1) - Ser69, Tyr27 (CDRH1) - Tyr57, Tyr27 - Asp34, Ser100 (CDRH3) - Asp30, Phe103 (CDRH3, main chain) - Thr73 and Gly104 (CDRH3, main chain) - Asp74 (Fig. 4*b*). On the other hand, Asp55 (CDRH2) forms a salt bridge with Lys211 from the Cκ domain of a different symmetry-related Fab, and together with Gly56 (CDRH2), packs against Pro117 and Ser118 (Fig. 4*c*).

The FabXol3 CDRH1 and CDRH3 conformations are markedly different to those in the FabXol, scFvXol and FabXol1 structures; the nature and implications of these conformational differences are discussed later.

3.7. Conformational diversity in the CDRs - comparison of unbound and bound Fab structures

In the FabXol, scFvXol, FabXol1[1] structures, and in molecules A and B of the FabXol1[2] structure, the heavy chain CDRs adopt similar conformations (Figs. 1*b*, 1*d*, 2*d* and 3*b*). However, substantial conformational diversity is observed for CDRH1 and CDRH3 in molecules C and D of the FabXol1[2] structure, and in FabXol3.

In molecules C and D of the FabXol1[2] structure, a glycerol molecule occupies a structurally equivalent position to Ser378 and Gly379 from the Cε3 domain in the complex between the omalizumab-derived Fab and IgE-Fc (Davies *et al*., 2017), altering the position of Tyr33 (CDRH1), which adopts a similar position to that in the IgE-Fc-bound Fab (Fig. 5*a*). The conformations of Ser31 (CDRH1) and Gly32 (CDRH1) are also similar to those in the complex, presumably due to the conformational change involving Tyr33. In the complex with IgE-Fc, Gly32 and Tyr33 from CDRH1 contribute to the interface with the Cε3 domain, packing against Ala377 and Ser378. The glycerol molecule, close to Tyr33, also causes the His101 (CDRH3) side chain to adopt a different position (Fig 5*a*); however, the overall conformation of CDRH3 is otherwise similar to that in the unbound FabXol, scFvXol, FabXol1[1] structures, and in molecules A and B of the FabXol1[2] structure.

In FabXol3, residues Ser25-Gly32 (CDRH1) adopt a markedly different conformation compared with the other unbound and bound Fab structures, which alters the positions of Tyr27 and Ile29; the Phe79 side chain, adjacent to CDRH1, also adopts a different position (Fig. 5*b*). On the other hand, Tyr33 adopts a similar position to that in molecules C and D of the FabXol1[2] structure, and the bound Fab

structures. Comparison of the FabXol3 structure with the structure of the complex with IgE-Fc (Davies *et al*., 2017) reveals that the position adopted by Ser25-Ser31, and Tyr33, in FabXol3 would not preclude an interaction with the Cε3 domain; however, Gly32 would clash with Ser378. This particular CDRH1 conformation thus appears to be incompatible with IgE binding. By contrast, in FabXol3, CDRH3 adopts a strikingly different conformation compared with the other Fab structures reported here (Fig. 5*c*). In these Fab structures, the CDRH3 conformation is incompatible with IgE binding due to steric clashes with the Cε3 domain. However, the CDRH3 conformation in the unbound FabXol3 structure is similar to the conformation adopted by CDRH3 in the FabXol3/IgE-Fc complex (Davies *et al*., 2017) (Fig. 5*d*); a conformational change in the CDRH3 main chain causes a dramatic rearrangement in the positions of side chain residues, particularly His101, Tyr102 and Phe103, which contact the Cε3 domain in the complex.

In contrast to the structural diversity displayed by CDRH1 and CDRH3, the conformation of CDRH2 is conserved in the unbound Fab and scFv structures, and in the complexes of the omalizumab Fab with the constrained Fcε3-4 molecule (Pennington *et al*., 2016), and FabXol3 with IgE-Fc (Davies *et al*., 2017). Like CDRH2, the light chain CDR conformations are also conserved; similar conformations are adopted in the twelve independent views reported here, and in other unbound Fab structures (Jensen *et al*., 2015; Wright *et al*., 2015), which are similar to those in the complexes between the omalizumab Fab and the constrained Fcε3-4 molecule (Pennington *et al*., 2016), and FabXol3 and IgE-Fc (Davies *et al*., 2017). Nevertheless, the FabXol2 and FabXol3 crystal structures show substantial conformational diversity in the heavy chain CDRs, and together with the FabXol1[2] structure, reveal how conformations compatible with IgE binding are adopted in the unbound Fab.

3.8. Interaction between the omalizumab-derived Fabs and scFv with IgE-Fc in solution

The aim of our mutagenesis strategy was to disrupt the crystal packing interactions observed in the wild-type omalizumab (FabXol) crystal structures, without mutating the CDR residues responsible for IgE-Fc binding, and significantly affecting the affinity for IgE-Fc. We have previously demonstrated that the kinetics of the interaction between omalizumab and IgE-Fc are biphasic, with one high-affinity (~1nM), and one lower-affinity (~30nM) interaction (Davies *et al*., 2017), and that FabXol3 has slightly higher affinity for IgE-Fc than FabXol (wild-type omalizumab Fab) and intact omalizumab (Davies *et al*., 2017).

We used surface plasmon resonance analysis to characterize further the interaction between IgE-Fc and the omalizumab-derived Fab and scFv constructs. As we have shown previously, at the highest concentration tested (100nM IgE-Fc), the omalizumab-derived Fabs and scFv all display the same mode of interaction with IgE-Fc, *i.e.* a biphasic model with one higher-affinity and one lower-affinity binding interaction (Davies *et al*., 2017). When these data were normalized to have the same maximum binding values, it was found that the association rates were similar to those for intact omalizumab (Davies *et al*., 2017; Table 5). However, a statistically significant trend of increasingly slower dissociation rates was observed: the dissociation rate for the omalizumab-derived Fab (FabXol) is slower than that for intact omalizumab, FabXol2 has a slower dissociation rate than FabXol, FabXol3 is even slower, while the scFvXol dissociation rate is the slowest of all (Table 5 and Supplementary Fig. S1).

4. Discussion

After unsuccessful attempts to crystallize the complex between the Fab fragment of the therapeutic anti-IgE omalizumab and IgE-Fc, and the Fcε3-4 region, we designed a mutagenesis strategy to disrupt the substantial, and recurring, crystal packing interactions observed in different omalizumab Fab structures. We targeted crystal packing interactions at two different interfaces. The first interface comprised hydrogen bonds between an edge β-strand from the Cγ1 domain (β-strand G, Lys214-Lys218) and a short segment of β-strand structure in the Cκ domain CD loop (Leu158-Ser160). The second interface involved the omalizumab heavy chain CDRs and V_L domain AB, C''D and EF loops and Cκ domain DE loop. Our mutations were designed to disrupt these packing interactions without significantly affecting the affinity of omalizumab for IgE, and as such, were distal to the antigen-binding CDRs.

Packing interactions similar to that between the Cγ1 domain edge β-strand (strand G) and the Cκ domain CD loop are found in a number of other crystal structures containing Fab fragments (e.g. Hall *et al*., 2016; Lee *et al*., 2017; Li *et al*., 2009; Sickmier *et al*., 2016). Indeed, a variety of packing interactions involving hydrogen bond networks between β-strands have been detected in crystal structures of intact antibodies and their fragments (Edmundson *et al*., 1999; Wingren et al., 2003), including anti-parallel arrangements between edge strands in Cλ and Cγ1 domains (*e.g*. Faber *et al*., 1998), V_H domains (*e.g*. Harris *et al*., 1998) and V_L domains (*e.g*. Bourne *et al*., 2002).

We mutated Leu158 from the omalizumab C_K domain CD loop to Pro (omalizumab-derived mutant FabXol1) to disrupt the interface with strand G from the Cγ1 domain, and although this was achieved,

the FabXol1 molecule still crystallized preferentially, in different packing arrangements stabilized in part by the presence of Pro158.

We next targeted the crystal packing interactions between the omalizumab CDRs and V_L and Cκ domain framework residues (V_L domain AB, C''D and EF loops and Cκ domain DE loop) from symmetry-related molecules. We mutated Ser81 and Gln83 from the omalizumab V_L domain EF loop to Arg, and created two omalizumab-derived mutants: FabXol2 contained the Ser81Arg and Gln83Arg mutations, while FabXol3 additionally contained the Leu158Pro mutation. The IgE-Fc protein was successfully crystallized in complex with both FabXol2 and FabXol3, and the 3.7Å resolution crystal structure of the FabXol3/IgE-Fc complex was recently reported (Davies *et al*., 2017). Engineering the Ser81Arg and Gln83Arg mutations in the V_L domain of the omalizumab Fab clearly disrupted the interactions seen in the FabXol structure, but these residues also formed new packing interactions in the FabXol2 and FabXol3 structures, seen when these molecules were crystallized alone. Presumably however, these packing contacts were collectively weaker than those in either FabXol or FabXol1, since they were unable to compete with the pre-formed Fab/IgE-Fc complexes and their crystallization.

Unbound IgE-Fc adopts an acutely bent conformation, in which the Cε2 domains fold back against the Fcε3-4 region (Doré *et al*., 2017; Holdom *et al*., 2011; Wan *et al*., 2002). IgE-Fc is more acutely bent in the crystal structure of the sFcεRIα/IgE-Fc complex (Holdom *et al*., 2011), less acutely bent when in complex with sCD23 (Dhaliwal *et al*., 2017), partially bent when in complex with FabXol3 (Davies *et al*., 2017), and fully extended in the complexes with the anti-IgE Fabs aεFab and 8D6 (Chen *et al*., 2018; Drinkwater *et al*., 2014); these structures demonstrate that IgE-Fc is conformationally dynamic. However, despite this flexibility, IgE adopts a predominantly bent conformation in solution (Beavil *et al*., 1995; Davis *et al*., 1990; Holowka & Baird, 1983; Holowka *et al*., 1985; Hunt *et al*., 2012; Zheng *et al*., 1991; Zheng *et al*., 1992). The propensity for IgE-Fc to adopt such a bent conformation might account for the selective crystallization of the omalizumab Fab and the omalizumab-derived mutant FabXol1. Bending of IgE-Fc, from the partially bent conformation observed in the FabXol3/IgE-Fc complex, to the acutely bent structure, would disrupt one of the omalizumab binding sites on the Cε3 domain. In the FabXol3/IgE-Fc complex, Arg81 and Arg83 from one FabXol3 molecule contact one of the Cε2 domains, in addition to the omalizumab binding site on the Cε3 domain. This additional interaction might stabilize the partially bent conformation in the complex.

In IgE-Fc and Fcε3-4, the Cε3 domains adopt a range of conformations relative to one another, from closed to open (Chen *et al*., 2018; Cohen *et al*., 2014; Davies *et al*., 2017; Dhaliwal *et al*., 2012; Dhaliwal *et al*., 2014; Dhaliwal *et al*., 2017; Doré *et al*., 2017; Drinkwater *et al*., 2014; Garman *et al*., 2000; Holdom *et al*., 2011; Jabs *et al*., 2018; Wan *et al*., 2002; Wurzburg & Jardetzky, 2009; Wurzburg *et al*., 2000; Yuan *et al*., 2013); this conformational diversity is crucial for the allosteric regulation of IgE binding to its receptors, FcεRI and CD23 (Borthakur *et al*., 2012; Dhaliwal *et al*., 2012). The flexibility of the Cε3 domains could account for our failure to crystallize the complex between the omalizumab Fab and the unconstrained Fcε3-4 molecule, which lacks the Cε2 domains. Notably, the reported omalizumab Fab complex (Pennington *et al*., 2016) is with an Fcε3-4 molecule that contains an engineered disulphide bond, which locks the Cε3 domains into a closed conformation, thus reducing the overall flexibility of the complex.

Fab fragments are invaluable tools as chaperone proteins for crystallization, and are used for their ability to trap different conformations or reduce flexibility in the target protein (Bukowska & Grütter, 2013; Griffin & Lawson, 2011; Rasmussen *et al*., 2007; Sun *et al*., 2018; Tamura *et al*., 2019; Uysal *et al*., 2009). However, in our case, crystallization trials of our conformationally flexible target protein, IgE-Fc, in complex with the Fab fragment of the therapeutic anti-IgE antibody omalizumab resulted in disruption of pre-formed complexes, and selective crystallization of the Fab alone.

Here we have described a successful mutagenesis strategy in which framework regions of the omalizumab Fab were engineered to disrupt recurring crystal packing interactions in the Fab crystal structures, without significantly altering the stability of the Fab, nor its affinity, for IgE-Fc. Although disrupting the hydrogen-bond mediated interactions between β-strands did not prevent selective crystallization of the Fab, the recurring interface between the light chain and CDRs was disrupted by introducing bulkier residues through point mutations in the light chain framework regions.

This approach, of introducing point mutations distal to the antigen-binding CDRs to disrupt undesired crystal packing interactions, could assist in the structure determination of Fabs in complex either with similarly conformationally flexible, or indeed inflexible, target proteins.

Acknowledgements We thank Dr. Anthony Keeble for helpful discussions. We thank Marty Rajaratnam (King's College London) for use of the in-house X-ray facility, and Diamond Light Source (Harwell, UK) for access to beamlines I02, I03, I04, I04-1 and I24 (proposal numbers

MX1220, MX7656 and MX9495) that contributed to the results presented here. We acknowledge the support of the Centre for Biomolecular Spectroscopy, King's College London. We thank Hanna Hailu for protein expression and Sue Cross, Sarfaraj Topia and Vidisha Krishnan for protein purification. T.C., J.T.H and A.J.H are employees of UCB Celltech. T.C. and A.J.H. are in receipt of stock options. A patent application has been filed based on elements of this work.

References

Adams, P.D., Afonine, P.V., Bunkóczi, G., Chen, V.B., Davis, I.W., Echols, N., Headd, J.J., Hung, L.W., Kapral, G.J., Grosse-Kunstleve, R.W., McCoy, A.J., Moriarty, N.W., Oeffner, R., Read, R.J., Richardson, D.C., Richardson, J.S., Terwilliger, T.C. & Zwart, P.H. (2010) *Acta Crystallogr. D Biol. Crystallogr*. **66**, 213-221.

Beavil, A.J., Young, R.J., Sutton, B.J. & Perkins, S.J. (1995) *Biochemistry* **34**, 14449-14461.

Borthakur, S., Hibbert, R.G., Pang, M.O., Yahya, N., Bax, H.J., Kao, M.W., Cooper, A.M., Beavil, A.J., Sutton, B.J., Gould, H.J. & McDonnell, J.M. (2012) *J. Biol. Chem*. **287**, 31457-31461.

Bourne, P.C., Ramsland, P.A., Shan, L., Fan, Z.C., DeWitt, C.R., Shultz, B.B., Terzyan, S.S., Moomaw, C.R., Slaughter, C.A., Guddat, L.W. & Edmundson, A.B. (2002) *Acta Crystallogr D Biol Crystallogr*. **58**, 815-823.

Bukowska, M.A. & Grütter, M.G. (2013) *Curr. Opin. Struct. Biol*. **23**, 409-416.

Chen, V.B., Arendall, W.B., Headd, J.J., Keedy, D.A., Immormino, R.M., Kapral, G.J., Murray, L.W., Richardson, J.S. & Richardson, D.C. (2010) *Acta Crystallogr. D Biol. Crystallogr*. **66**, 12-21.

Chen, J-B., Ramadani, F., Pang, M.O.Y., Beavil, R.L., Holdom, M.D., Mitropoulou, A.N., Beavil, A.J., Gould, H.J., Chang, T.W., Sutton, B.J., McDonnell, J.M. & Davies, A.M. (2018) *Sci. Rep.* **8**, 11548.

Cohen, E.S., Dobson, C.L., Käck, H., Wang, B., Sims, D.A., Lloyd, C.O., England, E., Rees, D.G., Guo, H., Karagiannis, S.N., O'Brien, S., Persdotter, S., Ekdahl, H., Butler, R., Keyes, F., Oakley, S., Carlsson, M., Briend, E., Wilkinson, T., Anderson, I.K., Monk, P.D., von Wachenfeldt, K., Eriksson, P.O., Gould, H.J., Vaughan, T.J. & May, R.D. (2014) *mAbs* **6**, 755-763.

Davies, A.M., Allan, E.G., Keeble, A.H., Delgado, J., Cossins, B.P., Mitropoulou, A.N., Pang, M.O.Y., Ceska, T., Beavil, A.J., Craggs, G., Westwood, M., Henry, A.J., McDonnell, J.M. & Sutton, B.J. (2017) *J. Biol. Chem*. **292**, 9975-9987.

Davis, K.G., Glennie, M., Harding, S.E. & Burton, D.R. (1990) *Biochem. Soc. Trans*. **18**, 935–936.

Dhaliwal, B., Pang, M.O.Y., Keeble, A.H., James, L.K., Gould, H.J., McDonnell, J.M., Sutton, B.J. & Beavil, A.J. (2017) *Sci. Rep*. **7**, 45533.

Dhaliwal, B., Pang, M.O.Y., Yuan, D., Beavil, A.J. & Sutton, B.J. (2014) *Acta Crystallogr. F Struct. Biol. Cryst. Commun*. **70**, 305-309.

Dhaliwal, B., Yuan, D., Pang, M.O., Henry, A.J., Cain, K., Oxbrow, A., Fabiane, S.M., Beavil, A.J., McDonnell, J.M., Gould, H.J. & Sutton, B.J. (2012) *Proc. Natl. Acad. Sci. USA* **109**, 12686-12691.

Doré, K.A., Davies, A.M., Drinkwater, N., Beavil, A.J., McDonnell, J.M. & Sutton, B.J. (2017) *Biochim. Biophys. Acta – Proteins and Proteomics* **1865**, 1336-1347.

Drinkwater, N., Cossins, B.P., Keeble, A.H., Wright, M., Cain, K., Hailu, H., Oxbrow, A., Delgado, J., Shuttleworth, L.K., Kao, M.W., McDonnell, J.M., Beavil, A.J., Henry, A.J. & Sutton, B.J. (2014) *Nat. Struct. Mol. Biol*. **21**, 397-404.

Edmundson, A.B., DeWitt, C.R., Goldsteen, B.Z. & Ramsland, P.A. (1999) *J. Crystal Growth* **196**, 276-284.

Emsley, P., Lohkamp, B., Scott, W.G. & Cowtan K. (2010) *Acta Crystallogr. D Biol. Crystallogr*. **66**, 486-501.

Evans, P.R. (2006) *Acta Crystallogr. D Biol. Crystallogr*. **62**, 72-82.

Evans, P.R. & Murshudov, G.N. (2013) *Acta Crystallogr. D Biol. Crystallogr*. **69**, 1204–1214.

Faber, C., Shan, L., Fan, Z., Guddat, L.W., Furebring, C., Ohlin, M., Borrebaeck, C.A.K. & Edmundson, A.B. (1998) *Immunotechnology* **3**, 253-270.

Fuh, G., Wu, P., Liang, W.C., Ultsch, M., Lee, C.V., Moffat, B. & Wiesmann C. (2006) *J. Biol. Chem*. **281**, 6625-6631.

Garman, S.C., Wurzburg, B.A., Tarchevskaya, S.S., Kinet, J-P. & Jardetzky, T.S. (2000) *Nature* **406**, 259-266.

Gould, H.J. & Sutton, B.J. (2008) *Nat. Rev. Immunol*. **8**, 205-217.

Griffin, L. & Lawson, A. (2011) *Clin. Exp. Immunol*. **165**, 285-291.

Hall, G., Cullen, E., Sawmynaden, K., Arnold, J., Fox, S., Cowan, R., Muskett, F.W., Matthews, D., Merritt, A., Kettleborough, C., Cruikshank, W., Taylor, D., Bayliss, R. & Carr, M.D. (2016) *J. Biol. Chem*. **291**, 16840-16848.

Harris, L.J., Skaletsky, E. & McPherson, A. (1998) *J. Mol. Biol*. **275**, 861-872.

Holdom, M.D., Davies, A.M., Nettleship, J.E., Bagby, S.C., Dhaliwal, B., Girardi, E., Hunt, J., Gould, H.J., Beavil, A.J., McDonnell, J.M., Owens, R.J. & Sutton, B.J. (2011) *Nat. Struct. Mol. Biol*. **18**, 571-576.

Holgate, S.T. (2014) *World Allergy Organ. J*. **7**, 17.

Holgate, S., Casale, T., Wenzel, S., Bousquet, J., Deniz, Y. & Reisner, C. (2005) *J. Allergy Clin. Immunol*. **115**, 459-465.

Holowka, D. & Baird, B. (1983) *Biochemistry* **22**, 3475-3484.

Holowka, D., Conrad, D.H. & Baird, B. (1985) *Biochemistry* **24**, 6260–6267.

Hunt, J., Keeble, A.H., Dale, R.E., Corbett, M.K., Beavil, R.L., Levitt, J., Swann, M.J., Suhling, K., Ameer-Beg, S., Sutton, B.J. & Beavil, A.J. (2012) *J. Biol. Chem.* **287**,17459-17470.

Jabs, F., Plum, M., Laursen, N.S., Jensen, R.K., Mølgaard, B., Miehe, M., Mandolesi, M., Rauber, M.M., Pfützner, W., Jakob, T., Möbs, C., Andersen, G.R. & Spillner, E. (2018) *Nat. Commun*. **9**, 7.

Jensen, R.K., Plum, M., Tjerrild, L., Jakob, T., Spillner, E. & Andersen, G.R. (2015) *Acta Crystallogr. F Struct. Biol. Cryst. Commun*. **71**, 419-426.

Kabsch, W. (2010) *Acta Crystallogr. D Biol. Crystallogr*. **66**, 125-132.

Krissinel, E. & Henrick, K. (2007) *J. Mol. Biol*. **372**, 774-797.

Lee, J.U., Shin, W., Son, J.Y., Yoo, K-Y. & Heo, Y-S. (2017) *Int. J. Mol. Sci*. **18**, 228.

Leslie, A.G.W. & Powell, H.R. (2007) *Evolving Methods for Macromolecular Crystallography* **245**, 41-51.

Li, S., Wang, H., Peng, B., Zhang, M., Zhang, D., Hou, S., Guo, Y. & Ding, J. (2009) *Proc. Natl. Acad. Sci. USA* **106**, 4349-4354.

McCoy, A.J., Grosse-Kunstleve, R.W., Adams, P.D., Winn, M.D., Storoni, L.C. & Read, R.J. (2007) *J. Appl. Cryst*. **40**, 658-674.

Murshudov, G.N., Skubák, P., Lebedev, A.A., Pannu, N.S., Steiner, R.A., Nicholls, R.A., Winn, M.D., Long, F. & Vagin, A.A. (2011) *Acta Crystallogr. D Biol. Crystallogr*. **67**, 355-367.

North, B., Lehmann, A. & Dunbrack, R.L. (2011) *J. Mol. Biol*. **406**, 228-256.

Pennington, L.F., Tarchevskaya, S., Brigger, D., Sathiyamoorthy, K., Graham, M.T., Nadeau, K.C., Eggel, A. & Jardetzky, T.S. (2016) *Nat. Commun*. **7**, 11610.

Rasmussen, S.G., Choi, H.J., Rosenbaum, D.M., Kobilka, T.S., Thian, F.S., Edwards, P.C., Burghammer, M., Ratnala, V.R., Sanishvili, R., Fischetti, R.F., Schertler, G.F., Weis, W.I. & Kobilka, B.K. (2007) *Nature* **450**, 383-387.

Sickmier, E.A., Kurzeja, R.J., Michelsen, K., Vazir, M., Yang, E. & Tasker, A.S. (2016) *PLoS One* **11**, e0163366.

Sun, J., Paduch, M., Kim, S.A., Kramer, R.M., Barrios, A.F., Lu, V., Luke, J., Usatyuk, S., Kossiakoff, A.A. & Tan, S. (2018) *Proc. Natl. Acad. Sci. USA* **115**, 10010-10015.

Sussman, G., Hébert, J., Barron, C., Bian, J., Caron-Guay, R.M., Laflamme, S. & Stern, S. (2014) *Ann. Allergy Asthma Immunol*. **112**, 170-174.

Tamura, R., Oi, R., Akashi, S., Kaneko, M.K., Kato, Y. & Nogi, T. (2019) *Protein Sci*. **28**, 823-836.

Uysal, S., Vásquez, V., Tereshko, V., Esaki, K., Fellouse, F.A., Sidhu, S.S., Koide, S., Perozo, E., Kossiakoff, A. (2009) *Proc. Natl. Acad. Sci. USA* **106**, 6644-6649.

Vagin, A. & Teplyakov, A. (1997) *J. Appl. Cryst*. **30**, 1022-1025.

Wingren, C., Edmundson, A.B. & Borrebaeck, C.A. (2003) *Protein Eng*. **16**, 255-264.

Wan, T., Beavil, R.L., Fabiane, S.M., Beavil, A.J., Sohi, M.K., Keown, M., Young, R.J., Henry, A.J., Owens, R.J., Gould, H.J. & Sutton, B.J. (2002) *Nat. Immunol*. **3**, 681-686.

Weatherill, E.E., Cain, K.L., Heywood, S.P., Compson, J.E., Heads, J.T., Adams, R. & Humphreys, D.P. (2012) *Protein Eng. Des. Sel*. **25**, 321-329.

Winn, M.D., Ballard, C.C., Cowtan, K.D., Dodson, E.J., Emsley, P., Evans, P.R., Keegan, R.M., Krissinel, E.B., Leslie, A.G., McCoy, A., McNicholas, S.J., Murshudov, G.N., Pannu, N.S., Potterton, E.A., Powell, H.R., Read, R.J., Vagin, A. & Wilson, K.S. (2011) *Acta Crystallogr. D Biol. Crystallogr*. **67**, 235-242.

Winter, G. (2010) *J. Appl. Cryst*. **43**, 186-190.

Wright, J.D., Chu, H-M., Huang, C-H., Ma, C., Chang, T.W. & Lim, C. (2015) *Sci. Rep*. **5**, 11581.

Wurzburg, B.A., Garman, S.C. & Jardetzky, T.S. (2000) *Immunity* **13**, 375-385.

Wurzburg, B.A. & Jardetzky, T.S. (2009) *J. Mol. Biol*. **393**, 176-190.

Young, R.J., Owens, R.J., Mackay, G.A., Chan, C.M., Shi, J., Hide, M., Francis, D.M., Henry, A.J., Sutton, B.J. & Gould, H.J. (1995) *Protein Eng*. **8**, 193-199.

Yuan, D., Keeble, A.H., Hibbert, R.G., Fabiane, S., Gould, H.J., McDonnell, J.M., Beavil, A.J., Sutton, B.J. & Dhaliwal, B. (2013) *J. Biol. Chem*. **288**, 21667-21677.

Zheng, L., Li, B., Qian, W., Zhao, L., Cao, Z., Shi, S., Gao, J., Zhang, D., Hou, S., Dai, J., Wang, H. & Guo, Y. (2008) *Biochem. Biophys. Res. Comm*. **375**, 619-622.

Zheng, Y., Shopes, B., Holowka, D. & Baird, B. (1991) *Biochemistry* **30**, 9125-9132.

Zheng, Y., Shopes, B., Holowka, D. & Baird, B. (1992) *Biochemistry* **31**, 7446–7456.

Table 1 Data processing and refinement statistics for FabXol[1], FabXol[2] and scFvXol.

Values for the outer shell are given in parentheses.

	FabXol[1]	FabXol[2]	scFvXol
Data processing			
Space group	P 2_1 2_1 2_1	P 1 2_1 1	P 3_1 2 1
a, *b*, *c* (Å)	65.38, 73.56,141.10	85.29, 73.57, 87.10	73.91, 73.91, 117.80
		β = 116.58°	
Resolution (Å):	65.38-1.85	77.89-2.30	64.01-2.30
	(1.89-1.85)	(2.42-2.30)	(2.38-2.30)
Completeness (%)	99.9 (99.9)	99.5 (96.9)	99.8 (99.9)
Multiplicity	7.2 (6.9)	3.7 (3.2)	5.5 (5.2)
Mean ((I)/σ(I))	4.3 (1.7)	9.0 (1.8)	6.2 (2.5)
$CC_{1/2}$	0.99 (0.413)	0.993 (0.631)	0.974 (0.597)
R_{pim}	0.078 (1.101)	0.060 (0.454)	0.121 (1.064)
R_{merge}	0.192 (2.641)	0.099 (0.674)	0.259 (2.248)
Wilson *B*-factor (Å^2)	22.8	44.0	24.6
Refinement			
R_{work} / R_{free} (%)[a]	16.77 / 19.03	18.78 / 22.58	17.80 / 20.62
No. of reflections	57 943	42 804	16 902
R.m.s. deviations			
Bond lengths (Å)	0.014	0.002	0.004
Bond angles (°)	1.334	0.535	0.683
Coordinate error (Å)	0.18	0.30	0.20
No. of atoms			
Protein	3 357	6 468	1751
Solvent	314	246	78
Other	70[b]	62[c]	14[d]
Ave. *B* factor (Å^2)			
Protein	27.81	47.55	33.68
Solvent	40.07	41.26	38.72

Other	51.82[b]	62.02[c]	53.20[d]
Ramachandran plot			
Favoured (%)	97.79	97.07	96.98
Allowed (%)	2.21	2.82	3.02

[a] R_{free} set comprises 5% of reflections

[b] 2-methyl-2,4-pentanediol, glycerol, phosphate

[c] ethylene glycol, polyethylene glycol, tris, sulfate

[d] polyethylene glycol

Table 2 Data processing and refinement statistics for FabXol1[1], FabXol1[2], FabXol2 and FabXol3. Values for the outer shell are given in parentheses.

	FabXol1[1]	FabXol1[2]	FabXol2	FabXol3
Data processing				
Space group	C 2 2 2_1	P 2_1 2_1 2_1	P 2_1 2_1 2_1	P 2_1 2_1 2_1
a, *b*, *c* (Å)	94.46, 116.84, 181.16	80.11, 162.04, 164.43	44.03, 96.61, 103.51	43.72, 96.25, 103.30
Resolution (Å):	47.23-1.80	82.21-2.50	28.08-2.05	33.37-1.45
	(1.83-1.80)	(2.55-2.50)	(2.11-2.05)	(1.53-1.45)
Completeness (%)	99.9 (99.9)	99.9 (99.8)	99.7 (96.3)	99.6 (97.6)
Multiplicity	10.0 (10.3)	6.7 (6.7)	7.5 (4.1)	6.8 (4.4)
Mean ((I)/σ(I))	15.9 (1.7)	8.9 (1.9)	7.5 (1.7)	14.8 (2.7)
$CC_{1/2}$	0.999 (0.596)	0.984 (0.562)	0.990 (0.608)	0.997 (0.832)
R_{pim}	0.031 (0.513)	0.105 (0.602)	0.075 (0.466)	0.031 (0.250)
R_{merge}	0.093 (1.572)	0.254 (1.464)	0.197 (0.889)	0.079 (0.475)
Wilson *B*-factor (Å^2)	26.8	13.2	17.4	11.2
Refinement				
R_{work} / R_{free} (%)[a]	16.76 / 19.22	21.23 / 23.88	17.35 / 22.14	16.60 / 18.36
No. of reflections	92 661	74 660	28 385	77 571
R.m.s. deviations				
Bond lengths (Å)	0.011	0.002	0.008	0.016
Bond angles (°)	1.148	0.529	0.954	1.482
Coordinate error (Å)	0.21	0.34	0.23	0.14
No. of atoms				
Protein	6 568	12 844	3 273	3 319
Solvent	498	299	304	341
Other	102[b]	128[c]	6[d]	51[e]
Ave. *B* factor (Å^2)				
Protein	32.47	36.23	23.11	19.36
Solvent	38.84	30.32	30.69	31.24
Other	56.02[b]	61.11[c]	45.81[d]	34.92[e]

Ramachandran plot				
Favoured (%)	97.62	97.12	97.70	98.22
Allowed (%)	2.38	2.88	2.30	1.78

[a] R_{free} set comprises 5% of reflections

[b] ethylene glycol, sulfate

[c] glycerol, polyethylene glycol, sulfate

[d] glycerol

[e] ethylene glycol, polyethylene glycol

Table 3 Nomenclature for the omalizumab-derived Fabs and scFv.

Construct	Sequence	Structure	No. of molecules in the asymmetric unit
FabXol	Wild type	FabXol[1]	1: FabXol[1]
		FabXol[2]	2: FabXol[2A], FabXol[2B]
FabXol1	Leu158Pro[a]	FabXol1[1]	2: FabXol1[1A], FabXol1[1B]
		FabXol1[2]	4: FabXol1[2A], FabXol1[2B], FabXol1[2C], FabXol1[2D]
FabXol2	Ser81Arg[a]	FabXol2	1: FabXol2
	Gln83Arg[a]		
FabXol3	Ser81Arg[a]	FabXol3	1: FabXol3
	Gln83Arg[a]		
	Leu158Pro[a]		
scFvXol	Wild type	scFvXol	1: scFvXol

[a] Mutation in the Fab light chain

[b] V_L and V_H domains are linked by a $(Gly_4Ser)_4$ linker

Table 4 Thermal stability of the omalizumab-derived Fabs.

	T_m (°C)
FabXol	79.9 ±0.5
FabXol1	79.0 ±0.7
FabXol2	77.1 ±0.5
FabXol3	78.8 ±0.4

Table 5 Kinetics of omalizumab, the omalizumab-derived Fabs and scFv binding to IgE-Fc.

Molecule immobilised	k_{on1} (M^{-1} s^{-1})	k_{on2} (M^{-1} s^{-1})	k_{off1} (s^{-1})	k_{off2} (s^{-1})
omalizumab	$3.3x10^{5}$	$2.9x10^{5}$	$7.0x10^{-4}$	$1.2x10^{-2}$
FabXol	$5.7x10^{5}$	$4.4x10^{5}$	$5.6x10^{-4}$	$1.2x10^{-2}$
FabXol2	$5.1x10^{5}$	$3.3x10^{5}$	$4.5x10^{-4}$	$1.1x10^{-2}$
FabXol3	$9.7x10^{5}$	$2.7x10^{5}$	$3.3x10^{-4}$	$9.0x10^{-3}$
scFvXol	$6.9x10^{5}$	$3.1x10^{5}$	$2.9x10^{-4}$	$8.7x10^{-3}$

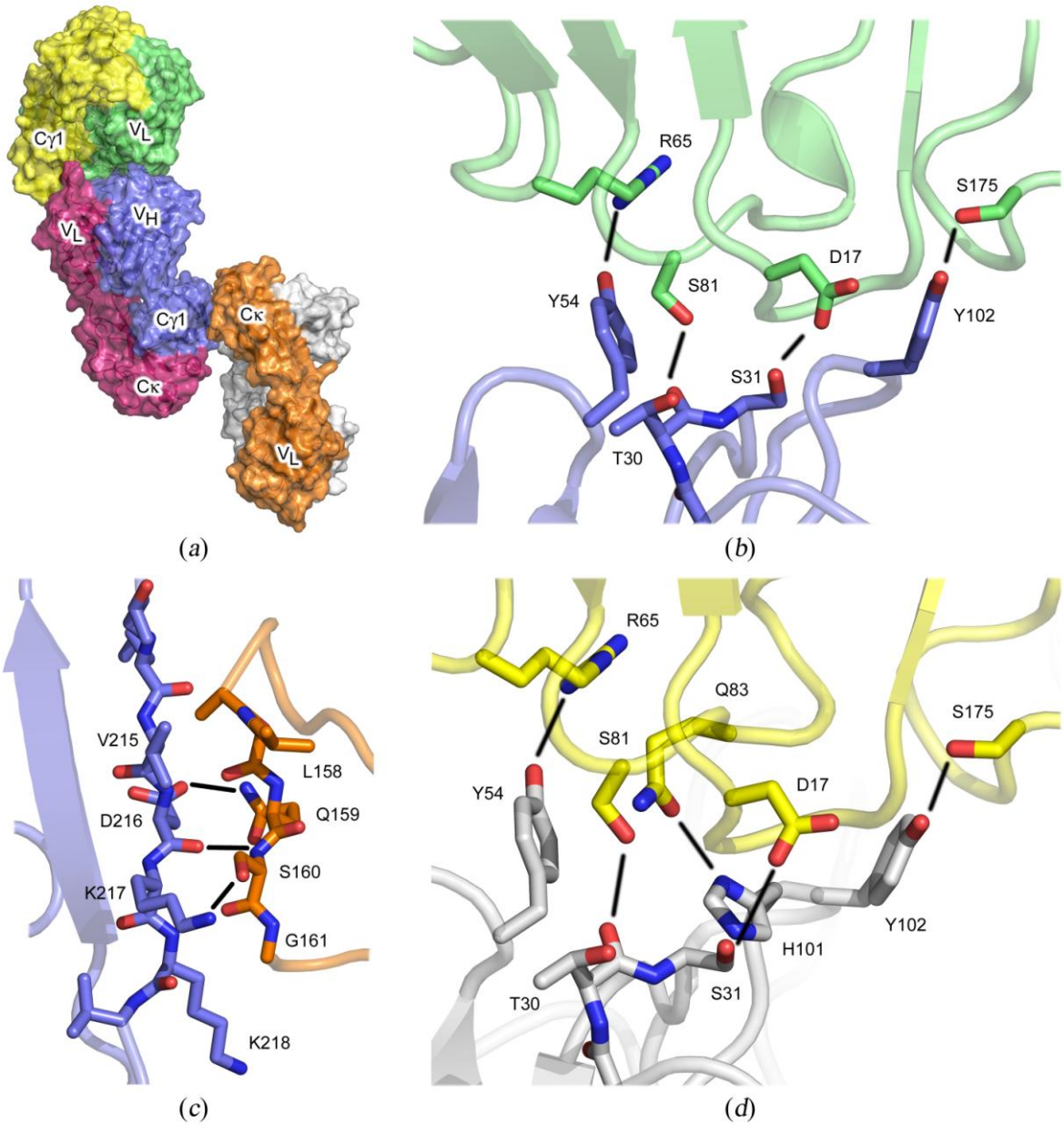

Figure 1 Structure of the omalizumab Fab (FabXol). (*a*) The FabXol[1] structure contains one Fab molecule (pink and blue) in the asymmetric unit. The heavy chain CDRs from this Fab contact the V_L and Cκ domains (the latter hidden in this view) from one symmetry-related molecule (green and yellow) and the Cκ domain from another (orange and gray). (*b*) Interface between heavy chain CDR residues (blue) and V_L and Cκ domain framework residues from a symmetry-related molecule (green) in the FabXol[1] structure. Hydrogen bonds are depicted by black lines. (*c*) Interface between an edge β-strand from the Cγ1 domain (blue) and the Cκ domain from a symmetry-related molecule (orange) in the FabXol[1] structure. Hydrogen bonds are depicted by black lines. (*d*) Interface between heavy chain CDR residues (gray) and V_L and Cκ domain framework residues from a symmetry-related molecule (yellow) for FabXol[2B], which includes a hydrogen bond between His101 (CDRH3) and Gln81 (V_L domain). Hydrogen bonds are depicted by black lines.

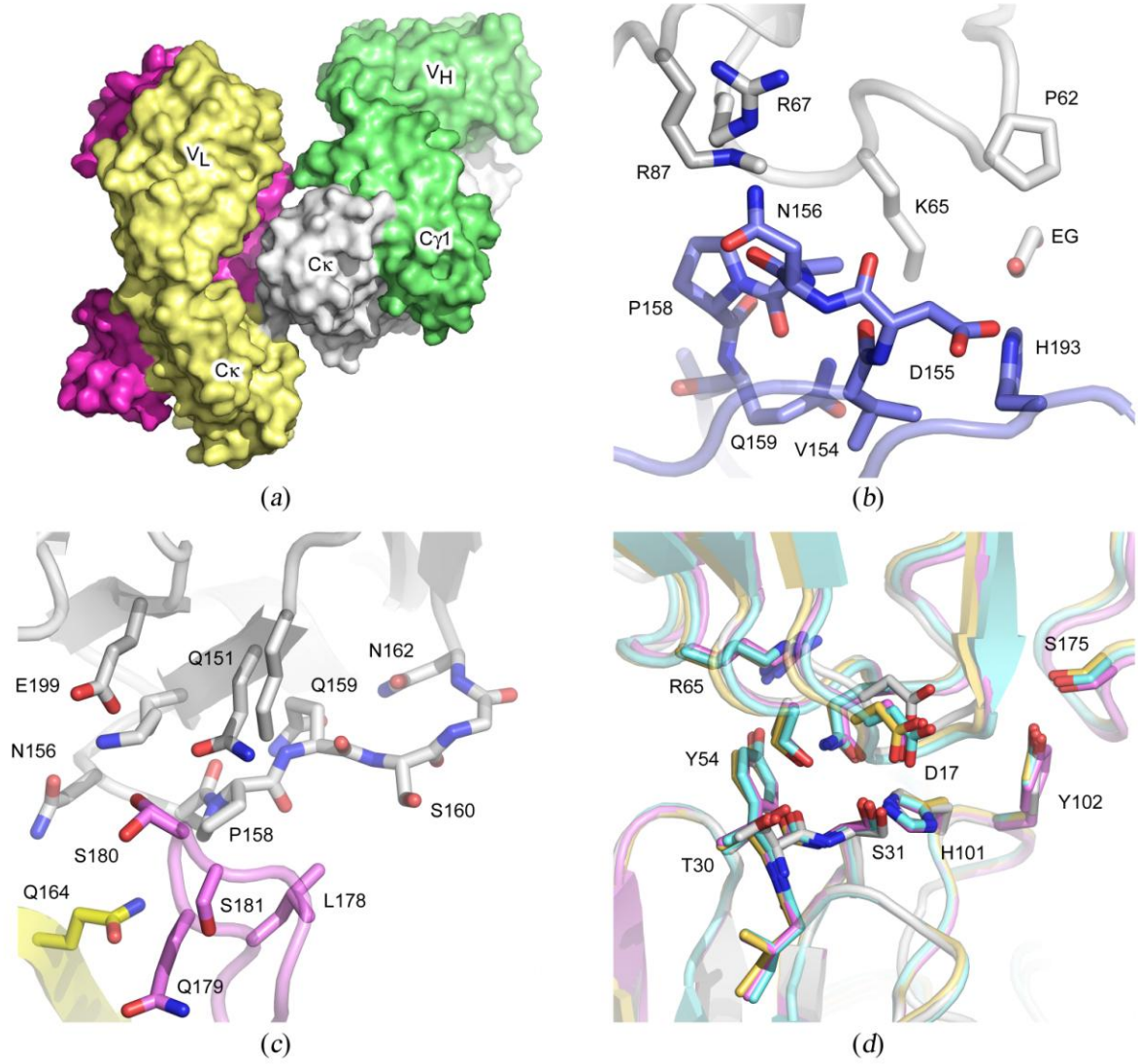

Figure 2 Structure FabXol1[1] for the omalizumab-derived Leu158Pro mutant (FabXol1). (*a*) The FabXol1[1] structure contains two molecules (pink and yellow / green and gray) in the asymmetric unit. (*b*) Interface between residues 155-159 from the Cκ domain (blue) of molecule FabXol1[1A] and the V_H domain of a symmetry-related molecule (gray). An ethylene glycol molecule (EG) is also bound at this interface. (*c*) Interface between the Cκ domain (gray) of molecule FabXol1[1B] and the Cκ domain (yellow) and Cγ1 domain (pink) of the non-crystallographic symmetry-related molecule, FabXol1[A]. (*d*) Conformations for CDRH1-3 residues, and their crystal packing interactions with the V_L domain (and Cκ domain in the Fabs), are similar for FabXol[1] (pink), FabXol1[1A] (yellow), FabXol1[1B] (blue) and scFvXol (gray).

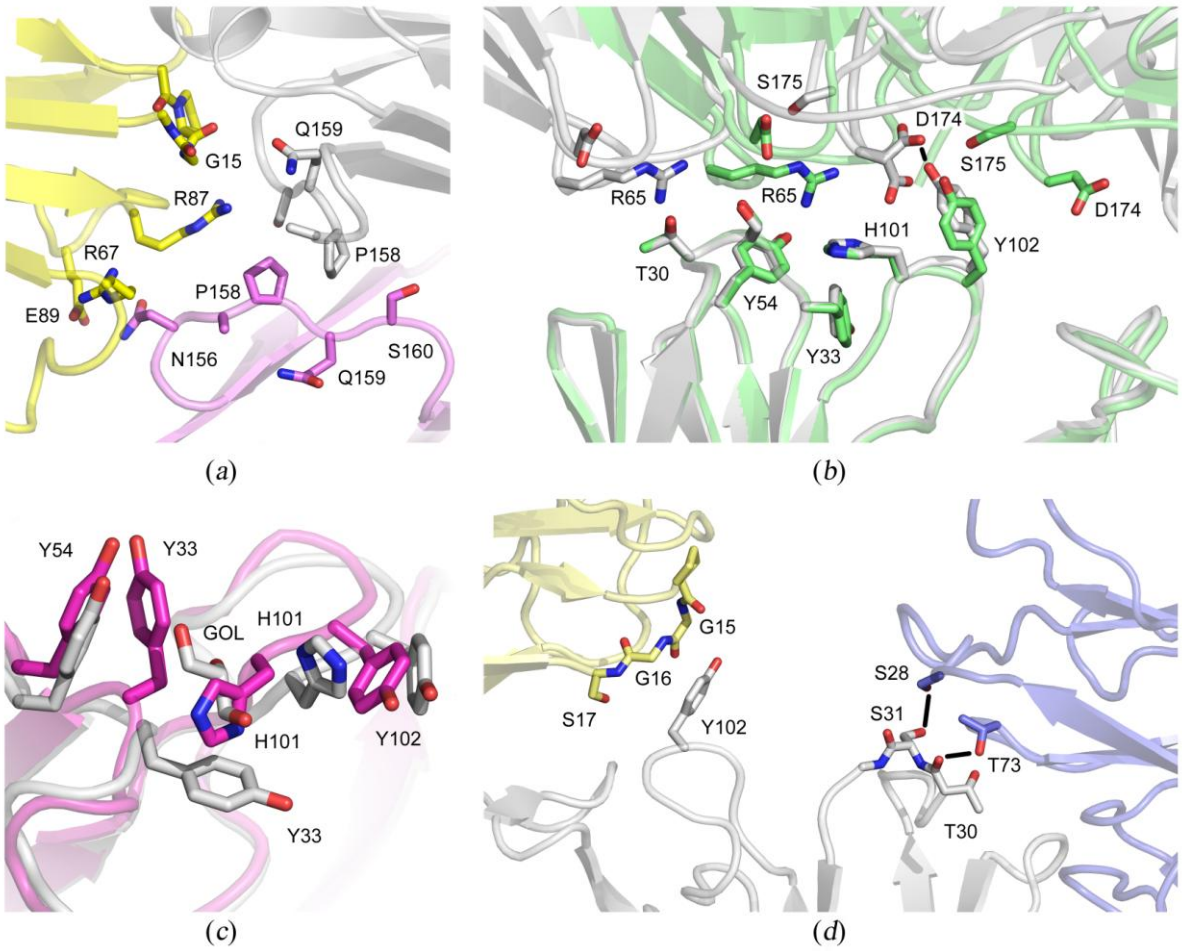

Figure 3 Structure FabXol1[2] for the omalizumab-derived Leu158Pro mutant (FabXol1). (*a*) In FabXol1[2C] (pink), residues Pro158-Ser160 form an interface with the Cκ domain from FabXol1[2A] (gray), and the V_H domain from FabXol1[2B] (yellow). (*b*) The FabXol1[2A] (gray) and FabXol1[2B] (green) CDRs adopt similar conformations, and both contact the V_L and Cκ domains from a symmetry-related molecule. A shift in the position of the symmetry-related molecule relative to FabXol1[2A] reduces the interface area, and only a single hydrogen bond is formed between Tyr102 (CDRH3) and Asp174 (Cκ domain). (*c*) Binding of a glycerol molecule (GOL) in FabXol1[2C] (gray) causes the Tyr33 and His101 side chains to adopt substantially different positions compared with those in FabXol1 (pink). (*d*) In FabXol1[2C] (gray), Thr30 and Ser31 form hydrogen bonds with Thr73 and Ser28, respectively, from a symmetry-related molecule (blue). Tyr102 packs against Gly15 and Gly16 from a different symmetry-related molecule (yellow).

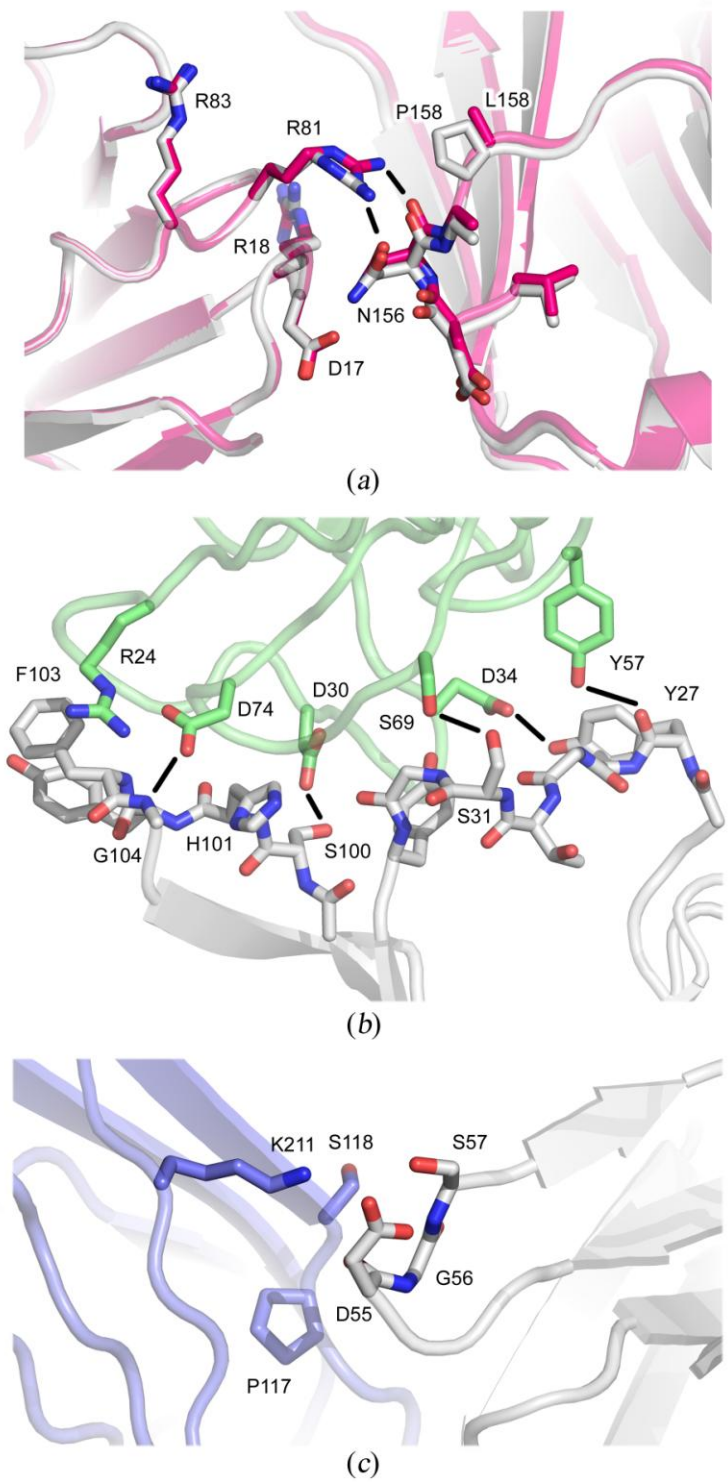

Figure 4 Structure of the omalizumab-derived Ser81Arg, Gln83Arg, Leu158Pro mutant (FabXol3). (*a*) In the FabXol3 (gray) and FabXol2 (pink) structures, Arg81 forms hydrogen bonds with Asn156. In the FabXol3 structure, Arg81 contacts Pro158, while Leu158 is partially disordered in the FabXol2 structure. Arg83 does not form any crystal packing interactions. (*b*) In the FabXol3 structure, CDRH1 and CDRH3 residues (gray) contact the V_L domain of a symmetry-related molecule (green). Hydrogen bonds are depicted by black lines. (*c*) Asp55 (CDRH2) forms a salt bridge with Lys211 from the Cκ domain of a symmetry-related molecule (blue).

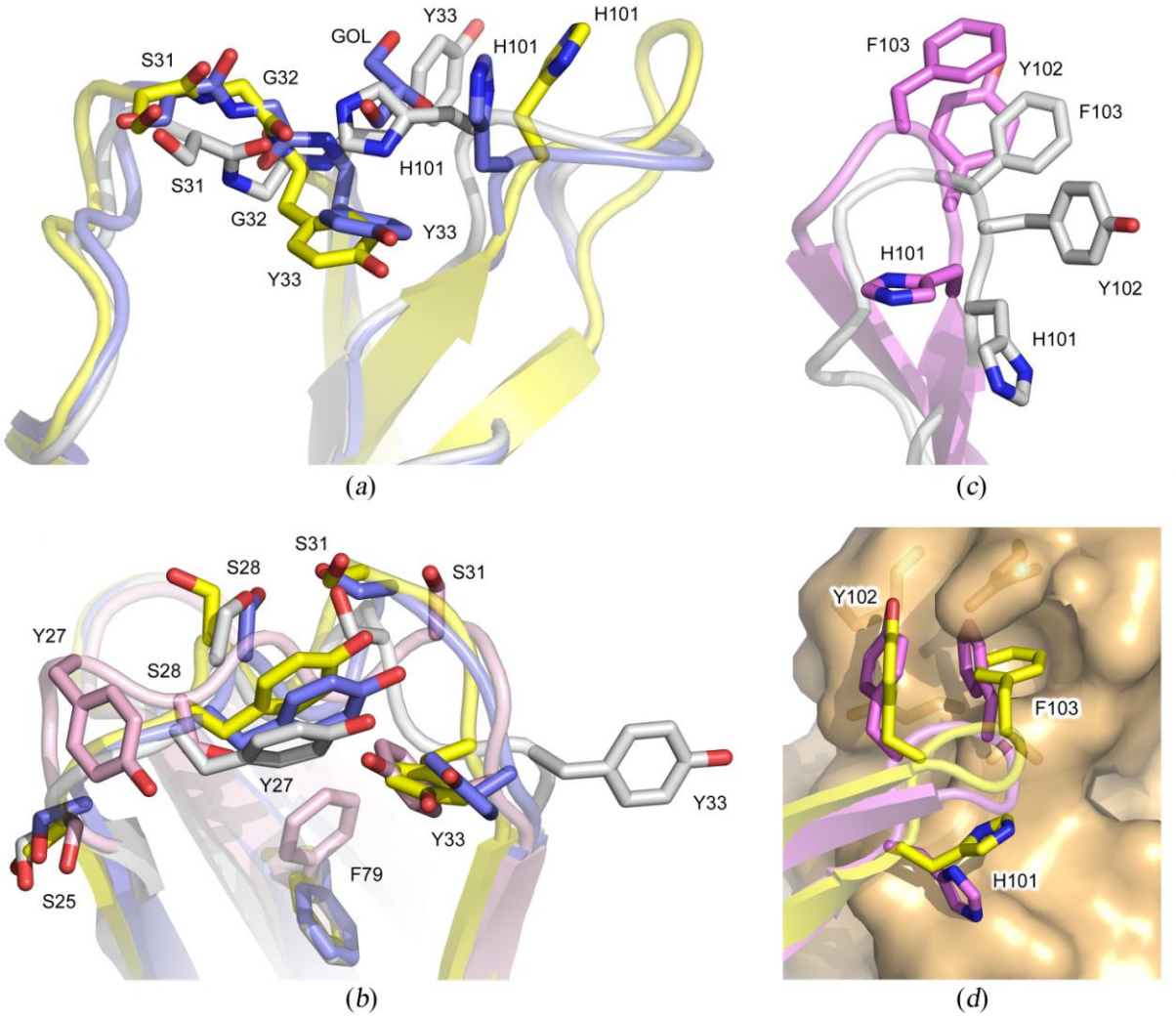

Figure 5 Conformational diversity in the omalizumab CDRs. (*a*) In molecule FabXol1[2C] (blue), binding of a glycerol molecule (GOL) alters the position of Tyr33 (CDRH1), which adopts a similar position to that in the IgE-Fc bound Fab (yellow) (Davies *et al.*, 2017). The FabXol[1] structure (gray) is shown for comparison. (*b*) Compared with the FabXol1 structure (gray), molecule FabXol1[2C] from the FabXol1[2] structure (blue), and FabXol3 from the complex with IgE-Fc (yellow), CDRH1 adopts a conformation in the unbound FabXol3 structure (pink) that alters the position of Tyr27 and Ile29 (CDRH1). Phe79 also adopts a different position. By contrast, Tyr33 (CDRH1) adopts a similar position in FabXol1[2C] (blue), unbound FabXol3 (pink) and FabXol3 bound to IgE-Fc (yellow). Tyr33 adopts a substantially different position in FabXol[1] (gray). (*c*) In the FabXol3 structure (pink), CDRH3 adopts a different conformation compared with that in the FabXol[1] structure (gray). (*d*) The conformation adopted by CDRH3 in the unbound FabXol3 structure (pink) is similar to that in the FabXol3/IgE-Fc complex (yellow). The surface of the Cε3 domain from the complex is colored orange (Davies *et al.*, 2017).

Supporting information

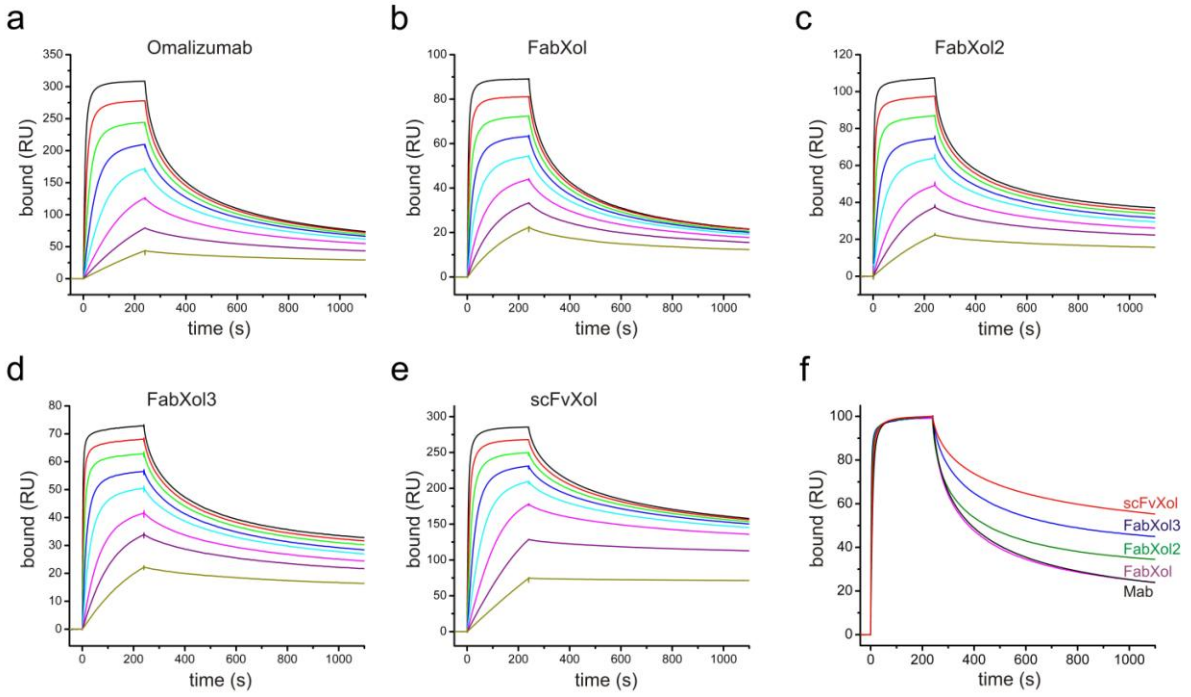

Figure S1 SPR sensorgrams of IgE-Fc binding to the following immobilized antibody constructs: (*a*) omalizumab, (*b*) FabXol (wild-type omalizumab Fab), (*c*) FabXol2, (*d*) FabXol3, and (*e*) scFvXol. IgE-Fc was injected over the surface at concentrations of 0.4nM (dark blue), 0.8nM (brown), 1.6nM (purple), 3.2nM (magenta), 6.4nM (cyan), 13nM (blue), 25nM (green), 50nM (red), and 100nM (black). (*f*) A comparison of normalized SPR measurements to assess the binding of 100nM IgE-Fc to omalizumab (Mab, black), FabXol (purple), FabXol2 (green), FabXol3 (blue), and scFvXol (red). The association rates of IgE-Fc to these different constructs are similar, but clear differences in off-rates can be observed.